Efficiency Enhancement of Aeroelastic Optimization Process Using Parametric Reduced-Order Modeling

Saeil Lee[1]; Taehyoun Kim[2]; and Shashank Srivastava[3]

Abstract: In this work, to demonstrate the efficiency of model reduction in design optimization, a parametric reduced-order model (PROM) was adopted in conjunction with an aeroelastic optimization process. Flutter speed was chosen as an objective function, and structural properties (material density, Young's modulus, and Poisson's ratio) as well as fluid properties (air density) were defined as the design variables. The flutter calculation was performed for a Goland wing, using finite-element modeling for the structure and the vortex lattice method for the aerodynamic part. A gradient-based optimization technique and a global optimization method were used to seek a maximum flutter speed. Comparison of optimization results from the full-order model (FOM) and PROM shows that the proposed optimization process yields the same optimum flutter speed as the FOM and yet reduces the computation time significantly, by up to a factor of four. **DOI: 10.1061/(ASCE)AS.1943-5525.0000805.**

Author keywords: Parametric reduced-order modeling; Flutter speed optimization; Aeroelasticity.

Introduction

Flutter is a rapid self-feeding motion resulting from a coupling between unsteady aerodynamic forces and structural vibrations. Structures subjected to fluid interactions are prone to this dynamic instability, which can induce a coupled fluid-structure resonance and subsequently lead to a structural failure. Static strength as well as dynamic behavior of the structure play key roles in its overall stability; hence, flutter analysis is usually done in the preliminary design phase. The knowledge of a critical flow condition at which flutter occurs is of utmost importance to the stability of the structure. Although the flow conditions around static structures such as bridges and buildings cannot be controlled, flow conditions can certainly be controlled for moving objects such as airplanes. Key parameters for wing design such as material properties, flight altitude, etc. can be optimized to curb flutter for a maximum flight velocity. Significant progress has been made in the last three decades in the field of design optimization of structures for optimization of wing/store configuration and flutter suppression. The traditional approach in aeroelastic optimization is minimization of structural mass subjected to buckling or flutter constraints. Turner (1969) and Rubin (1970) were among the first few to minimize the structural mass, keeping a specified flutter speed and structural frequency, respectively. This approach is still popular owing to design of light-weight aircraft in the modern aerospace industry. Stanford and Beran (2013a) used flutter speed as a minimum constraint and mass as a maximum constraint. Both approaches evolve the solution toward a maximum flutter speed and a minimum mass design. A more recent approach is to maximize the flutter speed by using structural parameters, such as mass, as design constraints.

Early mathematical programming methods used for structural optimization employed mixed direct or reciprocal design variables to get first-order approximations to objective functions and constraints. Morris (1982) built a sequence of approximated analytical models, each of them being optimized with a well-suited mathematical programming algorithm. Karpel (1992, 1999) proposed an approach that does not rely on analytical expressions to compute responses and sensitivities. Stanford and Beran (2011, 2013b) and De Leon and da Silva (2012) made notable contributions in the topological optimization of cantilevered wing structures for aeroelastic stability. However, the majority of research has been done assuming a fixed overall shape of the wing. Generally speaking, the structural mass should be minimized for flutter and critical load constraints. This intuitive proposition is very well backed up in literature. There are broadly two approaches of modeling minimum-mass structure. The first is the lumped mass consideration in which mass is treated to be concentrated at each panel center, and in the second the mass is considered to be distributed nonuniformly and is generally represented by a thickness distribution function, which is the ratio of panel thickness to uniform thickness of the reference. Early work in this area was given by Weisshaar (1972, 1976) and Pierson (1975), later followed by Van Keuren and Eastep (1977), Barboni et al. (1999), and Palaniappan et al. (2006).

In modern computational practices, continuous physical systems are discretized into finite spatial dimensions that are then usually stepped in the time domain to obtain a solution. Two examples of such modeling practices are finite-element analysis (FEA) and computational fluid dynamics (CFD). For flutter analysis of the wing, the aerodynamic envelope is discretized into grid-points, and a numerical solution is obtained by iterations until convergence is achieved. Such finite discretization of continuous systems generates very large-scale computational models. These full-order-models (FOMs), typically of the order of 10^5–10^7 [$O(10^5$–$10^7)$], are impractical for realistic applications because

[1]Research Fellow, Dept. of Mechanical Engineering, National Univ. of Singapore, 5 Engineering Dr. 2, Singapore 117579 (corresponding author). E-mail: mpelees@nus.edu.sg

[2]Associate Professor, Dept. of Mechanical Engineering, National Univ. of Singapore, 9 Engineering Dr. 1, Singapore 117576. E-mail: mpekimt@nus.edu.sg

[3]Ph.D. Student, Dept. of Mechanical Engineering, National Univ. of Singapore, 3 Engineering Dr. 2, Singapore 117578. E-mail: shashank.srivastava@u.nus.edu

Note. This manuscript was submitted on October 4, 2016; approved on July 13, 2017; published online on January 6, 2018. Discussion period open until June 6, 2018; separate discussions must be submitted for individual papers. This paper is part of the ***Journal of Aerospace Engineering***, © ASCE, ISSN 0893-1321.

they require large computer memories and excessively long CPU times to run the programs. Moreover, they are unsuitable for flutter stability analysis, which is usually done in the early design phase because of the complexity of the modeling as well as the large size. On the other hand, once constructed, reduced-order models (ROMs) $O(10^1–10^2)$ can successfully fulfill the engineering tasks, reducing the computational cost significantly and providing compact models for design purposes. Kim (2011) discussed the variety of model reduction methods available nowadays, especially in aeronautical applications including structural dynamics and aeroelasticity. Although ROM reduces the computational cost effectively, it cannot be adopted to an optimization process per se. This is because the conventional ROM is valid only for a certain parameter set, but during the optimization process they are constantly changed at every step. In the last decade, researchers have worked to resolve this issue and make the ROM adaptable to parameter changes. Frangos et al. (2010) gave a comprehensive overview of all the recent developments in the so-called reduced-order surrogate model (ROSM) techniques. Notable contributions have been made in recent years by Kholodar et al. (2003), Weickum et al. (2006), Amsallem and Farhat (2008), Zimmermann (2013), Paul-Dubois-Taine and Amsallam (2015), and Kim (1998, 2015, 2016). In particular, Kim developed a novel proper orthogonal decomposition (POD) technique for linear systems based on a frequency-domain formulation (Kim 2016) and use of the POD (Sirovich et al. 1990). In this method the system matrices are divided into a nominal and an incremental part, and the perturbed equation is converted to the so-called modally equivalent perturbed system (MEPS) in which the incremental matrices are isolated as a forcing term and no longer appear in the homogeneous part of the equation. This allows interpreting and analyzing the effects and impact of the parameter variations through the conventional ordinary differential equation with the forcing inputs.

In this work we combined the optimization process with the PROM developed by Kim (2016). To validate the accuracy and efficiency of the PROM, we performed two optimization techniques, namely the gradient-based method (GBM) and the genetic algorithm (GA), and maximize flutter speed as the objective function with respect to structural and aerodynamic parameters, i.e., mass, Young's modulus, Poisson's ratio, and air density. Air density was chosen as a design parameter to consider the altitude change during the flight. For simplicity of analysis, the Mach number was fixed at zero. The Goland wing model (Goland 1945) was used to describe dynamic behavior of the wing subject to the fluid-structure interaction. The first six modes were employed to represent the dynamics of the cantilevered wing. The wing was discretized into panels, and the vortex lattice method was used to generate unsteady aerodynamic equations. Generalized aerodynamic forces were calculated for the selected structural modes. The optimization results of the PROM and CPU time were compared with both an initial model and those of the FOM. The main goal of the study was to show that the PROM produces optimum flutter results that are identical to those by the FOM and yet the CPU time is significantly reduced, by as much as a factor of four for the wing model examined.

Problem Description and Numerical Approaches

Parametric Reduced-Order Modeling

The structural dynamic system can be described by a discrete-time, state-space equation

$$\boldsymbol{z}^{n+1} = \boldsymbol{A}_s\boldsymbol{z}^n + \boldsymbol{B}_s\boldsymbol{y}^n + \boldsymbol{B}_i\boldsymbol{u}^n \tag{1}$$

and similarly an unsteady aerodynamic model is given as

$$\boldsymbol{x}^{n+1} = \boldsymbol{A}_a\boldsymbol{x}^n + \boldsymbol{B}_a\boldsymbol{z}^n \tag{2}$$

$$\boldsymbol{y}^n = q_D(\boldsymbol{C}_a\boldsymbol{x}^n + \boldsymbol{D}_a\boldsymbol{z}^n) \tag{3}$$

where $\boldsymbol{x}$ = aerodynamic states vector; $\boldsymbol{y}$ = aerodynamic forces vector; $\boldsymbol{z}$ = structural states vector; $\boldsymbol{u}$ = inputs vector; q_D = dynamic pressure ($=\frac{1}{2}\rho V^2$); and subscripts s and a = structural and aerodynamic variables, respectively.

For a validation of finite-element modeling, natural frequencies of the first four modes of the Goland wing were computed and compared with the results reported previously by Beran et al. (2004) (Fig. 1). The unsteady flow field around the wing was modeled by the linear, inviscid vortex lattice model (Fig. 2) in the discrete-time, linear state-space format (Katz and Plotkin 1991; Hall 1994; Kim 2005), as described by Eqs. (2) and (3). Generalized aerodynamic forces (GAF) were calculated on the six structural modes and through the discrete-time Eqs. (2) and (3) were coupled with the structural dynamic Eq. (1), which is also cast in the state-space format. This resulted in a linear state-space aeroelastic system with 1,012 degrees of freedom, including 1,000 for the aerodynamics and $2 \times 6 = 12$ for the structure.

The $(1{,}012 \times 1{,}012)$ full-order model of the aeroelastic system is used for minimizing the objective function, i.e., negative flutter speed using a nonlinear multivariable programming solver in *MATLAB*. However, the FOM is computationally expensive because of its large size, and a ROM is desirable to reduce the size and computation. Toward this end, the following general first-order state-space equation subject to changes in parameters $\mu_i(i = 1,2, \ldots H)$ was considered:

$$\begin{aligned}\dot{\boldsymbol{x}}(\boldsymbol{\mu}, t) &= \boldsymbol{A}(\boldsymbol{\mu})\boldsymbol{x}(\boldsymbol{\mu}, t) + \boldsymbol{B}(\boldsymbol{\mu})\boldsymbol{u}(t)\ (N \times 1)\\ \boldsymbol{y}(\boldsymbol{\mu}, t) &= \boldsymbol{C}(\boldsymbol{\mu})\boldsymbol{x}(\boldsymbol{\mu}, t)\ (L \times 1)\end{aligned} \tag{4}$$

with lower and upper bounds on the parameters

$$\mu_{i1} \le \mu_i \le \mu_{i2},\ \text{nominal}\ (\mu_i) = \mu_{i0}(i = 1,2, \cdots, H) \tag{5}$$

To construct a ROM accounting for the changes in μ_i's, the FOM is first expanded and the parameters are split into nominal and perturbed parts as follows:

$$\begin{aligned}\boldsymbol{\mu} &= \boldsymbol{\mu}_0 + \boldsymbol{\Delta\mu}\\ \boldsymbol{x}(\boldsymbol{\mu}, t) &= \boldsymbol{x}_0(\boldsymbol{\mu}_0, t) + \boldsymbol{\Delta x}(\boldsymbol{\mu}, t)\\ \mathrm{A}(\mu) &= \mathrm{A}_0(\mu_0) + \Delta\mathrm{A}(\mu)\\ \mathrm{B}(\mu) &= \mathrm{B}_0(\mu_0) + \Delta\mathrm{B}(\mu)\\ \boldsymbol{C}(\boldsymbol{\mu}) &= \boldsymbol{C}_0(\boldsymbol{\mu}_0) + \boldsymbol{\Delta C}(\boldsymbol{\mu})\end{aligned} \tag{6}$$

where $\boldsymbol{x}_0, \boldsymbol{A}_0, \boldsymbol{B}_0, \boldsymbol{C}_0$ defined for $\boldsymbol{\mu}_0$ satisfy the nominal (or baseline) equation

$$\begin{aligned}\dot{\boldsymbol{x}}_0(t) &= \boldsymbol{A}_0\boldsymbol{x}_0(t) + \boldsymbol{B}_0\boldsymbol{u}(t)\\ \boldsymbol{y}_0(t) &= \boldsymbol{C}_0\boldsymbol{x}_0(t)\end{aligned} \tag{7}$$

and the perturbed system matrices $\boldsymbol{\Delta A}, \boldsymbol{\Delta B}$, and $\boldsymbol{\Delta C}$ are bounded as per Eq. (5). Expanding the system equation by inserting Eqs. (6) into (4) yields, after subtracting the nominal Eq. (7)

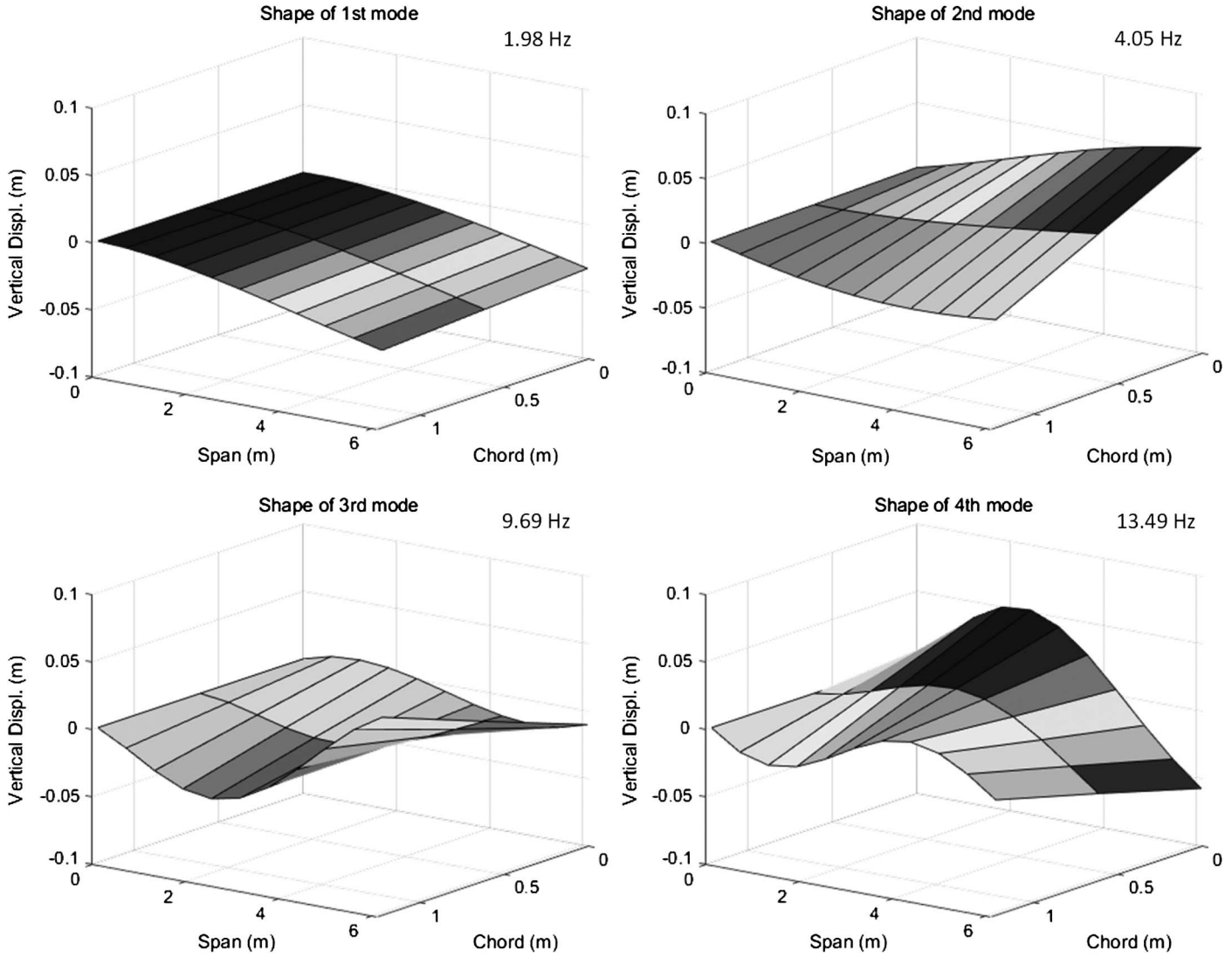

Fig. 1. Vibrational modes of Goland wing

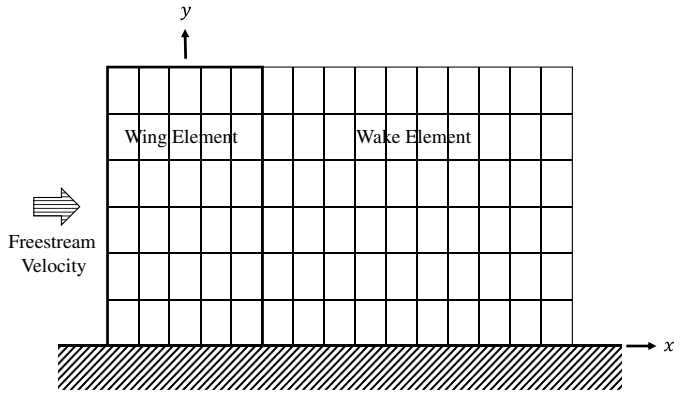

Fig. 2. Vortex lattice grids for rectangular semispan

$$\Delta\dot{x}(\mu,t) = [A_0 + \Delta A(\mu)]\Delta x(\mu,t) + \Delta A(\mu)x_0(t) + \Delta B(\mu)u(t) \tag{8}$$

Eq. (8) yields little insight into the effect of the variation on the dynamics of the perturbed system, and it is inefficient because ΔA is in the homogenous system matrix. Kim (2015) showed that, alternatively, the Eigen structure of the transfer function of the following equation can be examined:

$$\Delta\chi(\mu,\omega) = [j\omega I - A_0 - \Delta A(\mu)]^{-1}[\Delta A(\mu)\chi_0(\omega) + \Delta B(\mu)\mathcal{U}(\omega)] \tag{9}$$

The subspace spanned by the frequency responses of Eq. (9) is also spanned by the solutions of the MEPS

$$\Delta\chi'(\mu,\omega) = (j\omega I - A_0)^{-1}[\Delta A(\mu)\chi_0(\omega) + \Delta B(\mu)\mathcal{U}(\omega)] \tag{10}$$

that has isolated the incremental matrix ΔA out of the homogeneous part and into the forcing term. Hence, the frequency responses of Eqs. (9) and (10) span the same solution space, and it becomes preferable to sample Eq. (10) over Eq. (9). The time domain equation of (10) is

$$\Delta\dot{x}'(\mu,t) = A_0\Delta x'(\mu,t) + \Delta A(\mu)x_0(t) + \Delta B(\mu)u(t) \tag{11}$$

See Fig. 3 for the graphical conceptualization of the MEPS. The continuity in the parameters and hence in $\Delta A(\mu)$ and $\Delta B(\mu)$ is approximated with a few preselected ΔA_i's and ΔB_i's until a

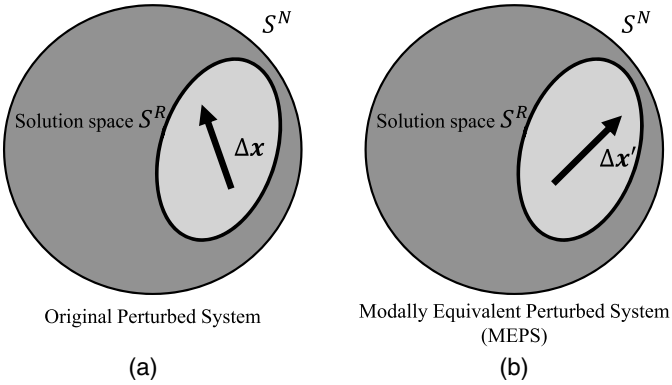

Fig. 3. Solution space (S^{R_1}) shared by (a) original and (b) modally equivalent perturbed solutions

convergence is met by checking ranks and singular value distributions of these matrices. See Kim (2015) for further details.

To find basis vectors of the solution space, samples or snapshots of the responses of the nominal system [Eq. (7)] and the MEPS [Eq. (10)] are taken and the output data is processed via the singular value decomposition (SVD). Only a few modes are retained, corresponding to the largest singular values. This process, known as the Karhunen-Loeve (KL) or the POD procedure, is well established in both the literature and practice for engineering applications (Sirovich et al. 1990). In this work, the snapshots are obtained in frequency domain via the frequency-domain Karhunen-Loeve procedure (FDKL) or frequency-domain POD (Kim 1998; Kim et al. 2004; Hall et al. 2000). The nominal Eq. (7) yields the mode set $\boldsymbol{\Phi}_0$ whereas the perturbed Eq. (10) yields the mode set $\boldsymbol{\Phi}_1$. Both sets of modes are combined to generate the total modal set $\boldsymbol{\Phi} \equiv [\boldsymbol{\Phi}_0 \boldsymbol{\Phi}_1]$. Assuming that R modes are retained, i.e., $\boldsymbol{\Phi} \equiv [\boldsymbol{\Phi}_1 \boldsymbol{\Phi}_2 \ldots \boldsymbol{\Phi}_R]$, the PROM is built by the approximation $\boldsymbol{x} \cong \boldsymbol{\Phi q}$ and applying Galerkin's projection

$$\begin{aligned} \boldsymbol{q}(\boldsymbol{\mu}, t) &= \boldsymbol{A}_R(\boldsymbol{\mu})\boldsymbol{q}(\boldsymbol{\mu}, t) + \boldsymbol{B}_R(\boldsymbol{\mu})\boldsymbol{u}(t) \\ \boldsymbol{y}(\boldsymbol{\mu}, t) &= \boldsymbol{C}_R(\boldsymbol{\mu})\boldsymbol{q}(\boldsymbol{\mu}, t) \end{aligned} \tag{12}$$

where

$$\begin{aligned} &\mathrm{A_R}(\mu) \equiv \Phi^{\mathrm{T}} \mathrm{A}(\mu) \Phi \ (\mathrm{R} \times \mathrm{R}) \\ &\mathrm{B_R}(\mu) \equiv \Phi^{\mathrm{T}} \mathrm{B}(\mu) \ (\mathrm{R} \times \mathrm{I}) \\ &\boldsymbol{C}_R(\boldsymbol{\mu}) \equiv \boldsymbol{C}(\boldsymbol{\mu})\boldsymbol{\Phi} \ (\mathrm{L} \times \mathrm{R}) \end{aligned} \tag{13}$$

such that Eq. (12) accurately reproduces results of the FOM [Eq. (4)] for any combination of the parameters in the range given in Eq. (5).

To recapitulate the advantages of the MEPS-based PROM, first, it is only necessary to solve the ordinary differential equation with forcing terms, Eqs. (10) or (11); second, the convergence is guaranteed when a sufficient number of $\boldsymbol{\Delta A_i}$'s, $\boldsymbol{\Delta B_i}$'s are included in the driving term of Eq. (10) such that the rank and singular value distribution of $[\boldsymbol{\Delta A}_1 \boldsymbol{\Phi}_0 \boldsymbol{\Delta B}_1 \boldsymbol{\Delta A}_2 \boldsymbol{\Phi}_0 \boldsymbol{\Delta B}_2 \ldots \boldsymbol{\Delta A}_K \boldsymbol{\Phi}_0 \boldsymbol{\Delta B}_K]$ converge; third, theoretically there is no limit on the amount of the deviations $\boldsymbol{\Delta A}(\boldsymbol{\mu})$ and $\boldsymbol{\Delta B}(\boldsymbol{\mu})$ because in linear analysis having an input of magnitude one has the same effect as having the same input of magnitude one million.

When the above procedure is applied to the Goland aeroelastic model described by Eqs. (1)–(3), it generates a (171×171) PROM (Kim 2015) that is valid for the entire range of the four parameters, and this is model was used in the flutter optimization process.

Problem Definition for Optimization

In this study, an optimization problem was defined with the four design variables and a single object function:

$$\begin{aligned} \text{Maximize } f(\boldsymbol{x}) &= v_f(\text{flutter speed}) \\ x &= [E, \nu, M, \rho_{\text{air}}] \\ \text{subject to } v_f - v_0 &> 0 \end{aligned}$$

where E = Young's modulus; ν = Poisson's ratio; M = mass; E, ν, and M vary in a half-quarter region of the wing (highlighted area in Fig. 4); and ρ_{air} = air density, which is a function of altitude. The flutter speed was selected for a constraint during this optimization process. The constraint was defined to exceed the initial flutter speed (v_0), that is, 91.44 m/s (300 ft/s), to avoid converging to the initial value. The optimization process was done by using an interior-point algorithm for finding the optima in gradient-based method cases. Simple description and the application of the interior-point algorithm are shown in the previous study from Jarre et al. (1998). A gradient-based method with a single starting point for a nonlinear optimization problem can only guarantee a local optimum. A local optimum can be a global optimum, but this cannot be guaranteed without checking the whole design space or using iterative gradient-based optimization process with a great enough number of different starting points. To ensure the global optimum, a global optimization method (heuristic method) such as genetic algorithm (GA) is used (Adeli and Cheng 1994).

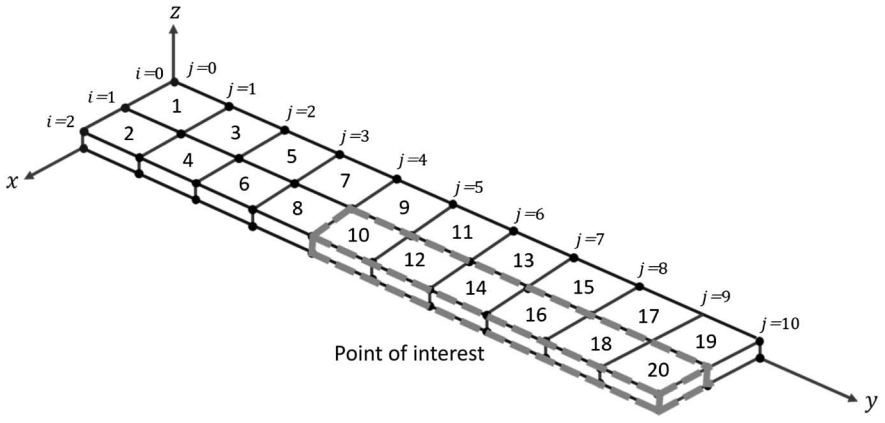

Fig. 4. Finite-element model of Goland wing

Table 1. Design Space for Flutter Speed Optimization

Design parameters	Lower	0	Upper
E ($\times 10^9$ kg/m^2)	0.8121	2.0305	3.2487
ν	0.20	0.33	0.45
M	−1	0	1
ρ_{air} (kg/m^3)	0.6530 [for 6,096 m (20,000 ft)]	0.9050 [for 3,048 m (10,000 ft)]	1.2251 (ground)

A heuristic method requires a significant amount of computation. Hence, applying a genetic algorithm to FOM system optimization is inefficient. To address this issue, the PROM was adopted to the optimization process. To check the efficiency, the genetic algorithm was performed with both the FOM and the PROM. Parameters and design space for optimization are defined in Table 1. Initial values of the three parameters for structure were selected from Kim (2015), and air density was defined with a cruise condition at 3,048 m (10,000 ft) of altitude. The mass on this Goland wing model was treated as lumped masses on the structural grids. The lumped masses were controlled with parameter M. The upper and lower boundaries were defined with certain ratios from initial values. For E, ν, and M, these boundaries were identical to the values used in Kim (2015), but the lower boundary of M was different from previous work; 40% of the initial value in this study. Boundaries on air density were defined for the different flight altitudes of 0 m (at ground) and 6,096 m (20,000 ft). A flowchart of the optimization process is shown in Fig. 5.

Flutter Speed Calculation

To find the flutter speed, the air speed was changed iteratively with an algorithm described in Fig. 6 until real parts of some of the aeroelastic eigenvalues became positive. In Fig. 6, ω_1 to ω_7 are the weight factors, which can be defined with trial and error. For validation, the flutter speed of the nominal case from the previous research (Kim 2015) was calculated using the current method. Fig. 7 shows convergence of the calculated flutter speed with this iterative calculation. It shows a well-matched result with the previous result from Kim's work (Kim 2015). The speed converged in about 15–20 iterations, although the number of iterations would vary for different parameter sets. Both the FOM and PROM yield the same flutter speed for the given design variables.

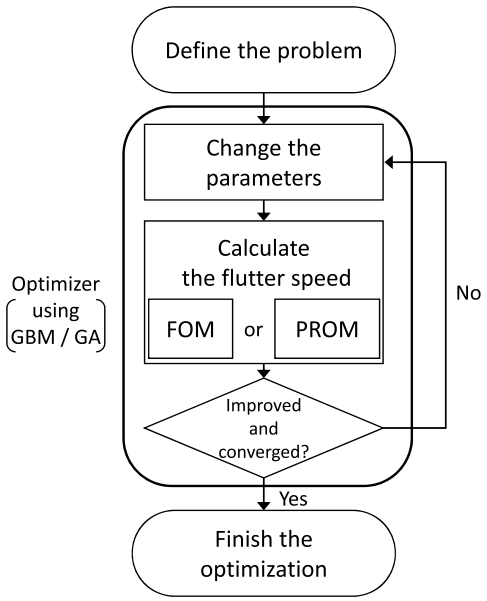

Fig. 5. Flowchart of the optimization procedure

Results

Model Description

The Goland wing is a benchmark model that many researchers in the aeronautical community have studied and used for the purpose of comparisons and validations of various structural and aeroelastic methods. The heavy Goland wing is modeled by the NASTRAN finite element (Fig. 4) (Beran et al. 2004). Nominal specs of the wing are given as follows:

$$l \equiv \text{span} = 6.096 \text{ m } (20 \text{ ft})$$

$$E \equiv \text{Young's Modulus} = 2.0305 \times 10^9 \text{ kg/m}^2 \quad (1.4976 \times 10^9 \text{ slugs/ft}^2)$$

$$c \equiv \text{Chord} = 1.2192 \text{ m } (4 \text{ ft})$$

$$\nu \equiv \text{Poisson Ratio} = 0.33$$

$$t \equiv \text{thickness} = 0.1006 \text{ m } (0.33 \text{ ft})$$

$$g \equiv \text{structural damping coefficient} = 0.03$$

In this study, structural design parameters were allowed to change in a quarter section of the wing. The changing section is highlighted in Fig. 4.

Result and Discussion

To check the accuracy of PROM in the process, flutter speed optimization was performed with both the FOM and PROM using the gradient-based method. For the gradient-based method cases, optimization was done using an interior point algorithm. The results are shown in Table 2. Parameters were normalized from −1 (lower bound) to 1 (upper bound) design spaces; and x1 is Young's modulus, x2 is Poisson's ratio, x3 is the parameter for lumped mass, and x4 is air density. The FOM and PROM converge to essentially the same optimal flutter speed. However, there was a substantial saving in the CPU time when switched to the PROM, by a factor of 3.5. For each iteration of the flutter speed estimation, the PROM took only 28.4% of the CPU time required for the FOM. Thus, total time for the gradient-based method with PROM was 41 minutes and 47 seconds, whereas the FOM took 2 h 27 min and 19 s using 1.7 GHz dual core CPU and 4GB RAM. Fig. 8 shows the convergence history. Both cases started from the same initial model and converged to the same optimum result with the identical path. The eigenvalues at the optimal flutter speed [$v_f = 193.7266$ m/s (635.5858 ft/s)] are shown in Fig. 9. This plot verifies that the PROM was constructed successfully and can substitute for the FOM in the optimization process.

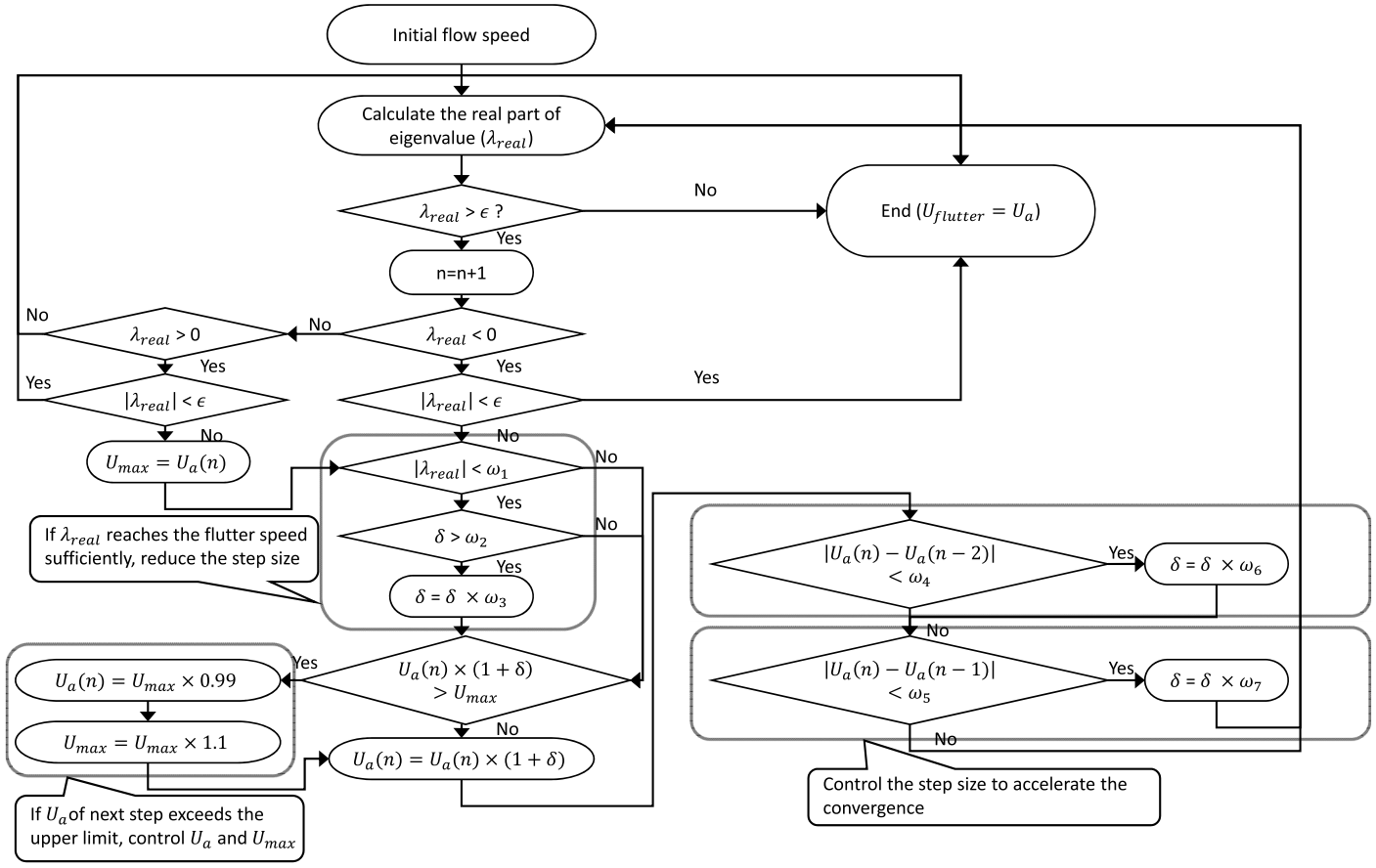

Fig. 6. Flutter speed estimation algorithm

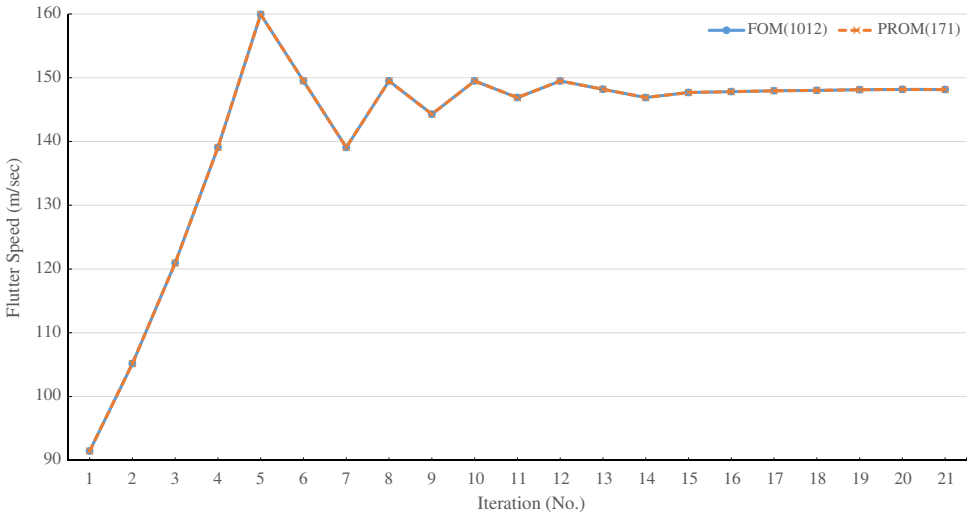

Fig. 7. Flutter speed estimation by iteration method

Table 2. Gradient Based Optimization Results of FOM and PROM

Cases	v_f	x1	x2	x3	x4	Time
GBM-PROM	193.7266	−0.8506	−0.8636	−0.9998	−0.9148	2,507.445 (00:41:47)
GBM-FOM	193.7266	−0.8506	−0.8636	−0.9998	−0.9148	8,839.482 (2:27:19)

Note: Air density: 0.6746 kg/m^3; lumped mass: −0.9998; Poisson's ratio: 0.2188; Young's modulus: 0.9942×10^9 kg/m^2.

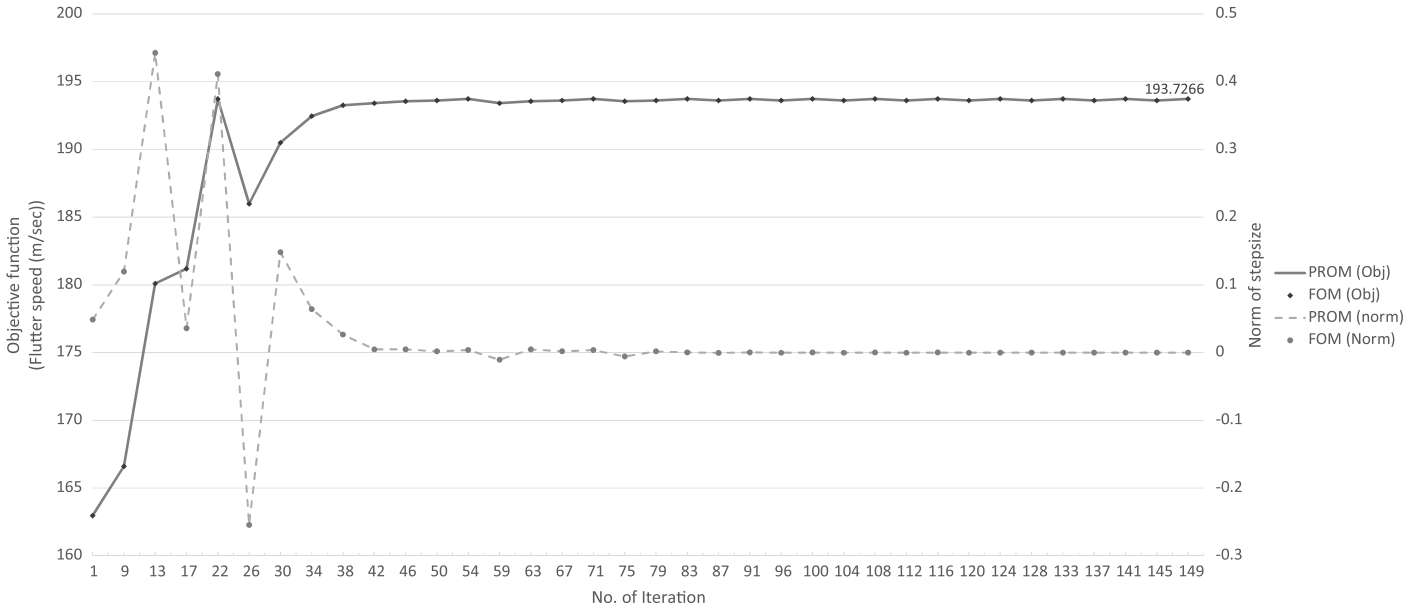

Fig. 8. Convergence history of GBM optimization using FOM and PROM

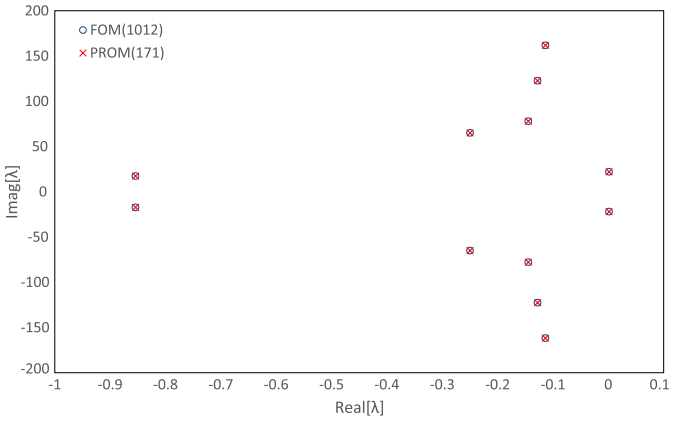

Fig. 9. Eigenvalues of FOM and PROM at $v_f = 193.73$ m/s

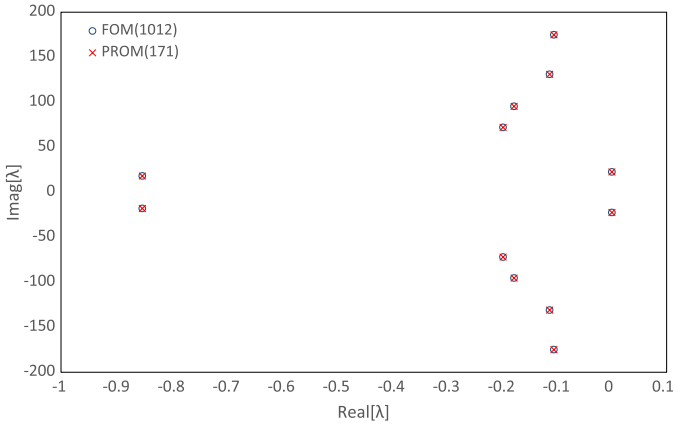

Fig. 10. Eigenvalues of FOM and PROM at $v_f = 197.71$ m/s

Table 3. Results of GA for PROM Case

Cases	v_f	x1	x2	x3	x4	Time
GA-PROM	197.7124	1.0	1.0	−1.0	−1.0	12,317.858 (3:25:18)
GA-FOM	197.7124	1.0	1.0	−1.0	−1.0	47,339.983 (13:09:00)

Note: Air density: 0.6530 kg/m^3; lumped mass: −1.0; Poisson's ratio: 0.45; Young's modulus: 3.2487×10^9 kg/m^2.

To confirm if the gradient-based method result is indeed global or not, a genetic algorithm method was used for the FOM and PROM cases. An initial population (set of the starting points with different parameter sets) for the genetic algorithm was 30, and a maximum generation of the genetic algorithm was 50 for the four parameters. In the genetic algorithm, every parameter set is calculated to get the value of the objective function at each generation. After getting the objective function values, the genetic algorithm performs basic operations, reproduction, cross-over, and mutation, and passes the new population to next generation (Adeli and Cheng 1994). The results of the genetic algorithm are shown in Table 3, and the eigenvalues are shown in Fig. 10. Comparing with the gradient-based results, the genetic algorithm optimization converged to a higher optimum point, implying that the gradient-based method produced a local optimum. The genetic algorithm with PROM and the genetic algorithm with FOM converged to the exact same flutter speed. The flutter speed has changed to 197.7124 m/s (648.66 ft/s), which is a 33.57% increase from the nominal flutter speed in previous research (Kim 2015). The genetic algorithm with the PROM took about 3 h 25 min, whereas the genetic algorithm with the FOM took about 13 h 9 min to converge. Hence, using the PROM saves 76.43% of the computation time. In the genetic algorithm–based optimization, all the parameters converged to either the lower or the upper boundaries of the range. This outcome is consistent with the physical intuition that a flutter would be optimized when the wing is lightest and stiffest simultaneously; a low mass and a low air density can reduce the inertial and aerodynamic forces in the wing, and a large Young's modulus and a high Poisson's ratio will make the wing more rigid. It also indicates that an even higher flutter speed could exist outside the specified boundaries. In this study, the optimization was unconstrained and had a single objective function. Thus, the design parameters naturally converged to the boundary values. If the boundaries were further

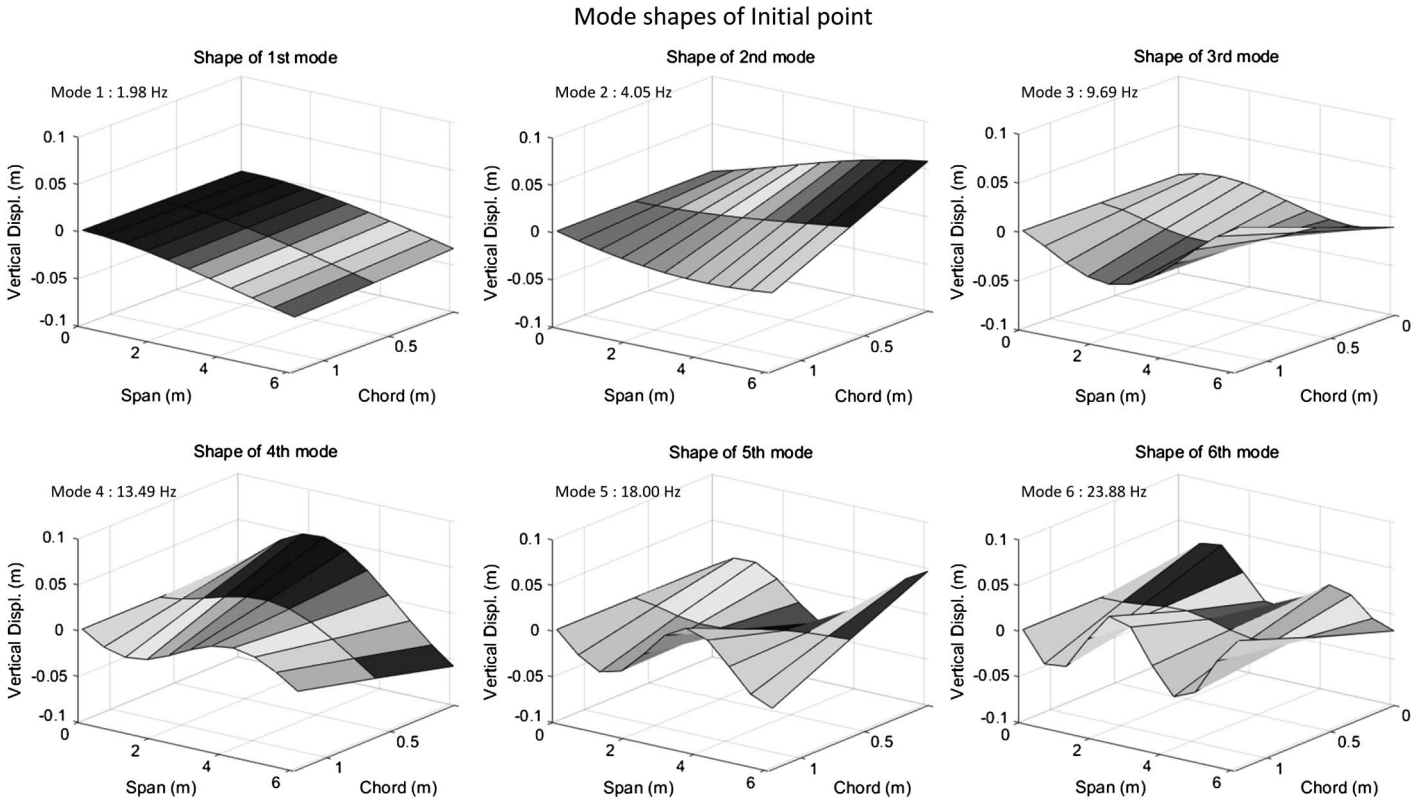

Fig. 11. Vibrational modes of the initial model

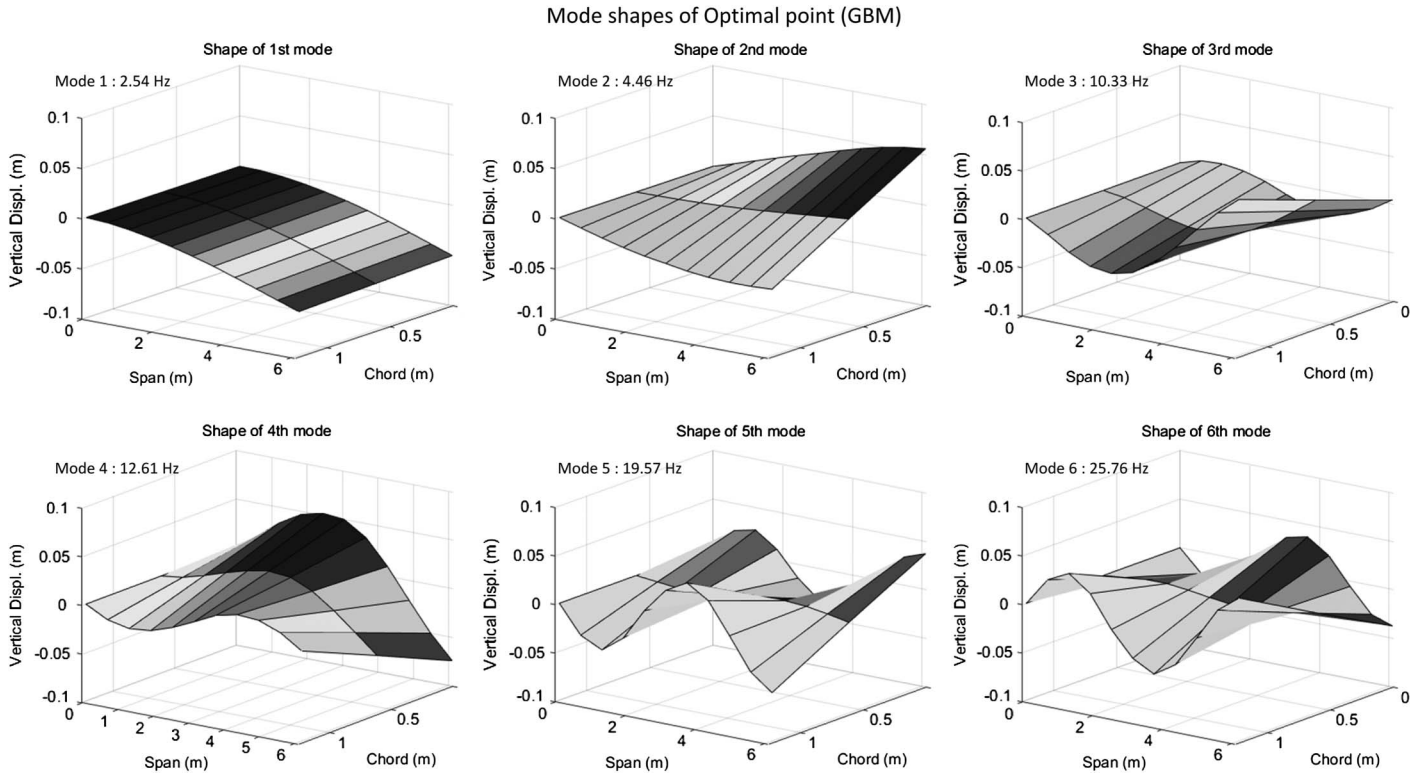

Fig. 12. Vibrational modes of the optimum model from GBM

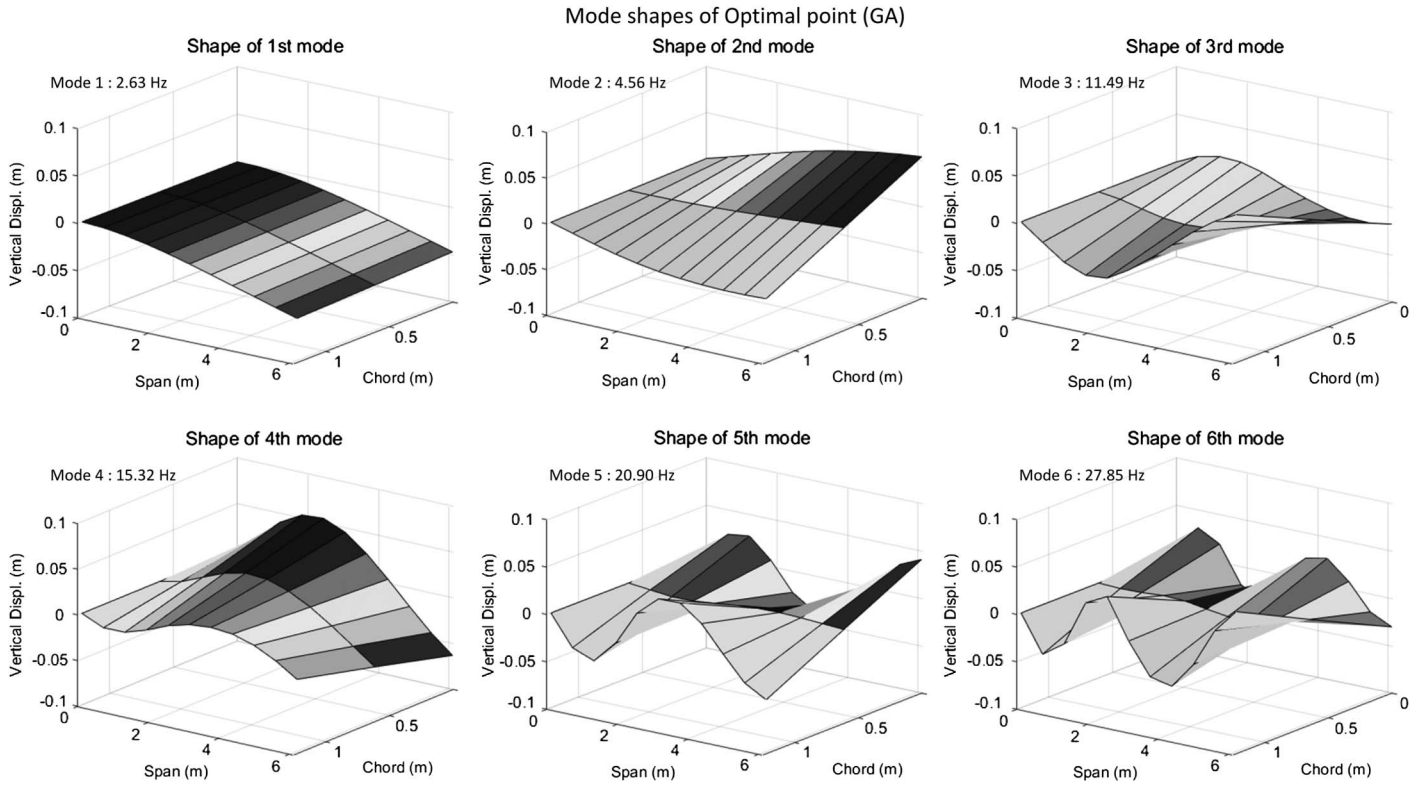

Fig. 13. Vibrational modes of the optimum model from GA

Table 4. Frequencies of Six Largest Modes

Frequency initial (Hz)	Frequency GBM (Hz)	Frequency GA (Hz)
1.981	2.538	2.626
4.049	4.456	4.563
9.686	10.334	11.493
13.492	12.605	15.323
18.001	19.571	20.896
23.877	25.760	27.855

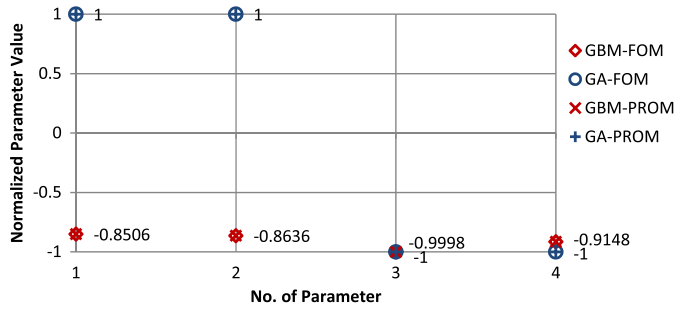

Fig. 14. Converged design parameters from GBM and GA optimization

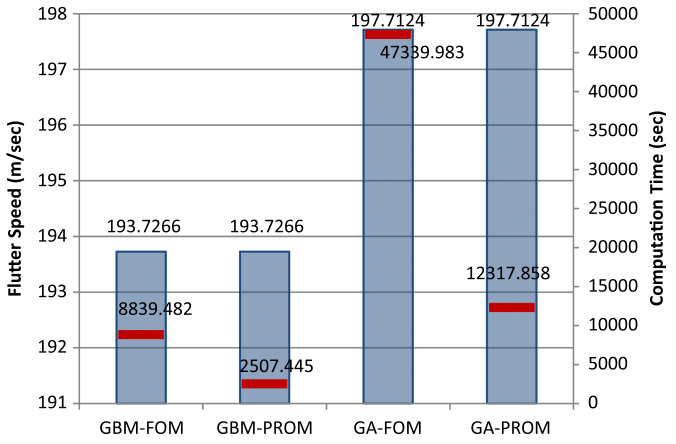

Fig. 15. Results of GBM and GA optimization

extended, the parameters would converge at the newer boundary values. A possible remedy for this problem is to define other structural objective functions or constraints such as maximum allowable bending moment or stress at the wing root.

Figs. 11–13 show the vibrational modes for the initial state, the optimum from the gradient-based method, and the optimum from the genetic algorithm parameter sets, respectively. Although the optimum mode shapes appear similar in magnitude and shape to those of the initial case, differences lie in frequencies of each mode. The frequencies are shown in Table 4. Fig. 14 shows the converged design parameters of the gradient-based method and genetic algorithm optimizations. The FOM and PROM results for the gradient-based method and genetic algorithm optimization match perfectly in this figure; x3 and x4 converged to similar values, but x1 and x2 converged to diametrically opposed values in the gradient-based method and genetic algorithm runs. This shows that the gradient-based method results are local optima, a premature solution on the path to the genetic algorithm result. The entire optimization results are shown graphically in Fig. 15. This figure summarizes the efficiency of adopting PROM in the optimization process.

Despite the significant reduction in the size of the PROM, from 1,012 to 171, the actual computing time was reduced by about 75%, less than what the reduced size would suggest. This is because in the optimization process, generating the inputs for structural and aerodynamic solver, calculating the mass and stiffness matrices, running the vortex lattice method, and so on all take extra time to estimate the flutter speed at each iteration.

Conclusion

In this paper, based on the parametric reduced-order model developed recently by Kim (2016), a new flutter optimization procedure was developed and successfully implemented. Although a traditional ROM is constructed for a specific parameter set and hence is not useful for optimization, a PROM can be used in the entire range of the design parameter space without having to execute the model reduction repeatedly. As a test case of the new optimization scheme, an objective function was defined to be the flutter speed and four design variables were introduced: material density, Young's modulus, Poisson's ratio, and air density. Both gradient-based and global optimization procedures were applied for validation. The result of the gradient-based optimization was 193.7266 m/s (635.5858 ft/s), taking about 2 h and 30 min for the FOM and 40 min for the PROM. The PROM result perfectly matched with that of the FOM but reduced the CPU time drastically. To ensure the global nature of the optimum result and check the effectiveness of the PROM on the heuristic method, the optimization was carried out again with a genetic algorithm. The flutter speed of the global optimum was increased to 197.7124 m/s (648.6627 ft/s), and it took 3 h and 25 min with the PROM and 13 h and 9 min with the FOM, respectively. Hence, the PROM reduces the computing time by a factor 4. It is expected that for more complex problems such as multidisciplinary design optimization (MDO), using PROM will prove to be even more effective resulting in significantly greater time savings in the computation.

Notation

The following symbols are used in this paper:

$\boldsymbol{A}, \boldsymbol{B}, \boldsymbol{C}$ = linear system or aeroelastic system matrices;
$\boldsymbol{A}_0, \boldsymbol{B}_0, \boldsymbol{C}_0$ = nominal system matrices;
$\boldsymbol{A}_R, \boldsymbol{B}_R, \boldsymbol{C}_R$ = reduced-order system matrices;
N = system dimension;
$\boldsymbol{q}$ = $(R \times 1)$ generalized coordinates for the PROM;
$\boldsymbol{q}_0$ = $(R_0 \times 1)$ generalized coordinates for the nominal system;
R = dimension of the PROM;
$\mathcal{U}$ = Fourier transform of $\boldsymbol{u}$;
$\boldsymbol{u}$ = (1×1) system inputs;
V = air speed;
v_f = flutter speed;
$\boldsymbol{x}$ = $(N \times 1)$ system states of aerodynamic states;
$\boldsymbol{x}_0$ = nominal solution of $\boldsymbol{x}$;
$\boldsymbol{y}$ = $(L \times 1)$ system outputs;
$\boldsymbol{\Delta A}, \boldsymbol{\Delta B}, \boldsymbol{\Delta C}$ = perturbed incremental system matrices;
$\boldsymbol{\Delta x}$ = perturbed solution of $\boldsymbol{x}$;
$\boldsymbol{\mu}$ = $(H \times 1)$ system parameters;
$\boldsymbol{\Phi}$ = $(N \times R)$ modes set for the PROM;
$\boldsymbol{\Phi}_0$ = $(N \times R_0)$ modes set for the nominal system;
$\boldsymbol{\Phi}_1$ = $(N \times R_1)$ modes set for the perturbed system; and
$\boldsymbol{\chi}$ = Fourier transform of $\boldsymbol{x}$.

References

Adeli, H., and Cheng, N. T. (1994). "Augmented Lagrangian genetic algorithm for structural optimization." *J. Aerosp. Eng.*, 10.1061/(ASCE)0893-1321(1994)7:1(104), 104–118.

Amsallem, D., and Farhat, C. (2008). "Interpolation method for adapting reduced-order models and application to aeroelasticity." *AIAA J.*, 46(7), 1803–1813.

Barboni, R., Mannini, A., and Gaudenzi, P. (1999). "On the use of the P-TFE method for panel flutter optimization." *Comput. Struct.*, 70(1), 109–117.

Beran, P. S., Khot, N. S., Eastep, F. E., Snyder, R. D., and Zweber, J. V. (2004). "Numerical analysis of store-induced limit-cycle oscillation." *J. Aircr.*, 41(6), 1315–1326.

De Leon, D. M., De Souza, C. E., Fonseca, J. S. O., and Da Silva, R. G. A. (2012). "Aeroelastic tailoring using fiber orientation and topology optimization." *Struct. Multidiscip. Optim.*, 46(5), 663–677.

Frangos, M., Marzouk, Y., Willcox, K., and van Bloemen Waanders, B. (2010). "Surrogate and reduced-order modeling: A comparison of approaches for large-scale statistical inverse problems." *Large-scale inverse problems and quantification of uncertainty*, Vol. 123149, Wiley, Chichester, U.K., 123–149.

Goland, M. (1945). "The flutter of a uniform cantilever wing." *J. Appl. Mech. Trans. ASME*, 12(4), A197–A208.

Hall, K. C. (1994). "Eigenanalysis of unsteady flows about airfoils, cascades, and wings." *AIAA J.*, 32(12), 2426–2432.

Hall, K. C., Thomas, J. P., and Dowell, E. H. (2000). "Proper orthogonal decomposition technique for transonic unsteady aerodynamic flows." *AIAA J.*, 38(10), 1853–1862.

Jarre, F., Kocvara, M., and Zowe, J. (1998). "Optimal truss design by interior-point methods." *SIAM J. Optim.*, 8(4), 1084–1107.

Karpel, M. (1992). "Multidisciplinary optimization of aeroservoelastic systems using reduced-size models." *J. Aircr.*, 29(5), 936–946.

Karpel, M. (1999). "Reduced-order models for integrated aeroservoelastic optimization." *J. Aircr.*, 36(1), 146–155.

Katz, J., and Plotkin, A. (1991). *Low-speed aerodynamics: From wing theory to panel methods*, McGraw-Hill, New York.

Kholodar, D. B., Thomas, J. P., Dowell, E. H., and Hall, K. C. (2003). "Parametric study of flutter for an airfoil in inviscid transonic flow." *J. Aircr.*, 40(2), 303–313.

Kim, T. (1998). "Frequency-domain Karhunen-Loeve method and its application to linear dynamic systems." *AIAA J.*, 36(11), 2117–2123.

Kim, T. (2005). "Efficient reduced-order system identification for linear systems with multiple inputs." *AIAA J.*, 43(7), 1455–1464.

Kim, T. (2011). "System identification for coupled fluid-structure: Aerodynamics is aeroelasticity minus structure." *AIAA J.*, 49(3), 503–512.

Kim, T. (2015). "Surrogate model reduction for linear dynamic systems based on a frequency domain modal analysis." *Comput. Mech.*, 56(4), 709–723.

Kim, T. (2016). "Parametric model reduction for aeroelastic systems: Invariant aeroelastic modes." *J. Fluids Struct.*, 65(Aug), 196–216.

Kim, T., Nagaraja, K. S., and Bhatia, K. G. (2004). "Order reduction of state-space aeroelastic models using optimal modal analysis." *J. Aircr.*, 41(6), 1440–1448.

MATLAB [Computer software]. MathWorks, Natick, MA.

Morris, A. J. (1982). *Foundation of structural optimization: A unified approach*, Wiley, London.

Palaniappan, K., Beran, P. S., and Jameson, A. (2006). "Optimal control of LCOs in aerostructural systems: Having your (nonlinear) cake and eating it too." *Proc., 47th AIAA/ASME/ASCE/AHS/ASC Structures, Structural Dynamics, and Materials Conf.*, AIAA, Newport, RI.

Paul-Dubois-Taine, A., and Amsallem, D. (2015). "An adaptive and efficient greedy procedure for the optimal training of parametric reduced-order models." *Int. J. Numer. Methods Eng.*, 102(5), 1262–1292.

Pierson, B. L. (1975). "Panel flutter optimization by gradient projection." *Int. J. Numer. Methods Eng.*, 9(2), 271–296.

Rubin, C. P. (1970). "Minimum weight design of complex structures subject to a frequency constraint." *AIAA J.*, 8(5), 923–927.
Sirovich, L., Kirby, M., and Winter, M. (1990). "An eigenfunction approach to large scale transitional structures in jet flow." *Phys. Fluids A: Fluid Dyn.*, 2(2), 127–136.
Stanford, B., and Beran, P. (2011). "Optimal structural topology of a plate-like wing for subsonic aeroelastic stability." *J. Aircr.*, 48(4), 1193–1203.
Stanford, B., and Beran, P. (2013a). "Aerothermoelastic topology optimization with flutter and buckling metrics." *Struct. Multidiscip. Optim.*, 48(1), 149–171.
Stanford, B., and Beran, P. (2013b). "Direct flutter and limit cycle computations of highly flexible wings for efficient analysis and optimization." *J. Fluids Struct.*, 36(Jan), 111–123.
Turner, M. J. (1969). "Optimization of structures to satisfy flutter requirements." *AIAA J.*, 7(5), 945–951.
Van Keuren, G. M., and Eastep, F. E. (1977). "Use of Galerkin's method for minimum-weight panels with dynamic constraints." *J. Spacecraft Rockets*, 14(7), 414–418.
Weickum, G., Eldred, M., and Maute, K. (2006). "Multi-point extended reduced order modeling for design optimization and uncertainty analysis." *Proc., 47th AIAA/ASME/ASCE/AHS/ASC Structures, Structural Dynamics, and Materials Conf. (2nd AIAA Multidisciplinary Design Optimization Specialist Conf.)*, AIAA, Newport, RI.
Weisshaar, T. A. (1972). "Aeroelastic optimization of a panel in high Mach number supersonic flow." *J. Aircr.*, 9(9), 611–617.
Weisshaar, T. A. (1976). "Panel flutter optimization—A refined finite element approach." *Int. J. Numer. Methods Eng.*, 10(1), 77–91.
Zimmermann, R. (2013). "Gradient-enhanced surrogate modeling based on proper orthogonal decomposition." *J. Comput. Appl. Math.*, 237(1), 403–418.